

Separation of a Breast Cancer Cell Line from Human Blood Using a Quadrupole Magnetic Flow Sorter

Masayuki Nakamura,[†] Keith Decker,[†] Julia Chosy,[†] Kristin Comella,[†] Kristie Melnik,^{†,‡} Lee Moore,[§] Larry C. Lasky,^{‡,||} Maciej Zborowski,[§] and Jeffrey J. Chalmers^{*,†,⊥}

Department of Chemical Engineering, The Ohio State University, 125 Koffolt Laboratories, 140 West 19th Avenue, Columbus, Ohio 43210, Department of Pathology, The Ohio State University, Columbus, Ohio 43210, Department of Biomedical Engineering, The Cleveland Clinic Foundation, 9500 Euclid Avenue, Cleveland, Ohio 44195, and Richard M. Ross Cord Blood Bank, American Red Cross, Columbus, Ohio 43205

We have developed a quadrupole magnetic flow sorter (QMS) to facilitate high-throughput binary cell separation. Optimized QMS operation requires the adjustment of three flow parameters based on the immunomagnetic characteristics of the target cell sample. To overcome the inefficiency of semiempirical operation/optimization of QMS flow parameters, a theoretical model of the QMS sorting process was developed. Application of this model requires measurement of the magnetophoretic mobility distribution of the cell sample by the cell tracking velocimetry (CTV) technique developed in our laboratory. In this work, the theoretical model was experimentally tested using breast carcinoma cells (HCC1954) overexpressing the HER-2/neu gene, and peripheral blood leukocytes (PBLs). The magnetophoretic mobility distribution of immunomagnetically labeled HCC1954 cells was measured using the CTV technique, and then theoretical predictions of sorting recoveries were calculated. Mean magnetophoretic mobilities of $(1-3) \times 10^{-4} \text{ mm}^3/(\text{T A s})$ were obtained depending on the labeling conditions. Labeled HCC1954 cells were mixed with unlabeled PBLs to form a "spiked" sample to be separated by the QMS. Fractional recoveries of cells for different flow parameters were examined and compared with theoretical predictions. Experimental results showed that the theoretical model accurately predicted fractional recoveries of HCC1954 cells. High-throughput (3.29×10^5 cells/s) separations with high recovery (0.89) of HCC1954 cells were achieved.

Introduction

The separation of rare cells (less than 1%) from heterogeneous cell suspensions is desired for a variety of clinical and biological applications. A majority of these applications can be divided into two categories: (1) depletion of an undesired cell(s) from a population of desired cells or (2) positive selection of a rare cell for further analysis or clinical use. An example of the first category is the depletion of residual tumor burden cells from bone marrow or stimulated apheresis product (Shammo et al., 1999). Examples of the second category include detection/removal of epithelial (cancer) cells from circulating blood for diagnostic and prognostic purposes (Racila et al., 1998), removal of fetal cells from maternal circulation (Mavrou et al., 1998), and selection of specific peptide fractions from a polypeptide library expressed on the surface of a bacterium (Daugherty et al., 1999).

The two major cell separation technologies currently in use are fluorescence-activated cell scanning/sorting

(FACS) and magnetic cell separation. The primary advantage of FACS is the possibility of multidimensional gating based on differences in cell size, granularity, and type or degree of fluorescence. However, this technique is limited by a relatively slow sorting rate (typically 1×10^3 to 1×10^4 cells/s) and color compensation issue when multicolor fluorescent antibodies are used (Hoffman and Houck, 1997; Shapiro, 1995).

A major advantage of magnetic cell separation is the simplicity of the design and operation of the sorting devices. To date, batch operations of commercially available magnetic sorting devices have focused on the enrichment of rare cells. Enrichment of leukocyte subsets (B-cells, T-cells, natural killer cells, etc.) is an example of the more popular application (Safarik and Safarikova, 1999). Recently, enrichment of carcinoma (epithelial tumor) cells in the blood from cancer patients has been attempted, in which initial ratios of target carcinoma cells were in the range of $1/10^4$ to $1/10^7$. For example, Bilkent et al. (2001) applied the MACS system (Miltenyi Biotech, Bergisch Gladbach, Germany) to enrich carcinoma cells (HEA-positive cells) in peripheral blood from renal carcinoma patients. They succeeded in reducing the cell sample size to one slide for immunocytochemical analysis. Iinuma et al. (2000) also used the MACS system to detect circulating tumor cells from colorectal cancer patients. They immunomagnetically labeled leukocytes

* To whom correspondence should be addressed. Phone: (614) 292-2727. Fax: (614) 292-3769. E-mail: chalmers.1@osu.edu.

[†] Department of Chemical Engineering, The Ohio State University.

[‡] Department of Pathology, The Ohio State University.

[§] The Cleveland Clinic Foundation.

^{||} American Red Cross.

[⊥] Director, University Cell Analysis and Sorting Core.

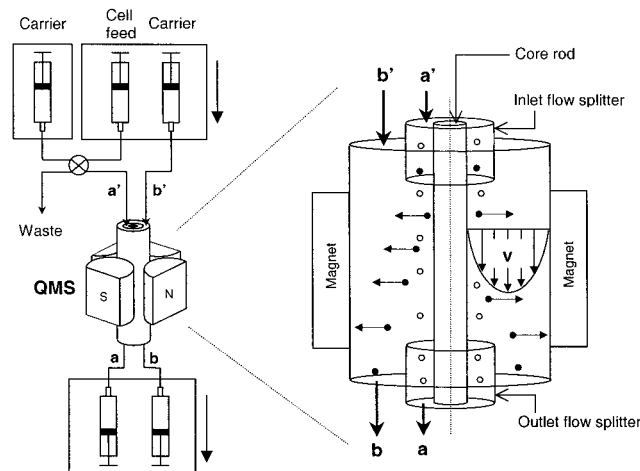


Figure 1. Schematic diagram of the QMS. The cell sample was fed from inlet a' and binary sorted to outlets a (negative fraction) and b (positive fraction).

(CD45-positive cells) for depletion to perform accurate RT-PCR detection of tumor cells. Gauthier et al. (2001) used Dynabeads (Dynal, Oslo, Norway) to enrich epithelial cancer cells (BerEP4-positive cells) in the blood of cancer patients, followed by (TRAP)-ELISA to measure telomerase activity.

We have developed two novel "flow-through" devices in our laboratories, the quadrupole magnetic flow sorter (QMS) (Sun et al., 1998; Chalmers et al., 1998; Zborowski et al., 1999) and the dipole magnetic flow sorter (DMFS) (Moore et al., 1998). The QMS was designed specifically for high-throughput cell separations, whereas the DMFS was designed to fractionate positively labeled cells into subfractions on the basis of their differences in mobility. The potential throughput of the QMS is expected to be 10^6 to 10^7 cells/s, which is higher than those of FACS and batch magnetic cell separation. In addition to high-throughput cell sorting, other advantages of the QMS are the feasibility of scale-up and the relatively low cost.

A schematic drawing of the QMS is shown in Figure 1. The cell suspension is fed from the inlet (a') by a syringe pump. The cells are subjected to a magnetic energy gradient in the annular flow channel, resulting in the migration of immunomagnetically labeled cells toward the outer wall. At the outlet, the cells are sorted into depleted (a) and enriched (b) fractions.

We have reported that CD4-, CD8-, and CD45-positive subpopulations immunomagnetically labeled with antibodies conjugated to colloidal magnetic beads were separated from leukocyte samples using the QMS (Sun et al., 1998; Chalmers et al., 1998). Results as good as 99% purity and 86% recovery (separate experiments) of positively labeled cells were achieved. However, the labeling and separating conditions used in these experiments were semiempirically optimized, limiting the efficiency of the sorting process.

To overcome the inefficiency of semiempirical operation/optimization, a theoretical model of QMS sorting was developed. The theoretical determinants of the sorting outcome are (1) the magnetophoretic mobility distribution of the cell sample, (2) the annular flow channel geometry, (3) the strength of the magnetic energy gradient, and (4) the adjustable flow parameters (Williams et al., 1999). When these four conditions are given, the model predicts a cell trajectory within the separator that results in one of three possible sorting outcomes: (1) stream a, (2) stream b, or (3) retention on the outer wall. This model has been the basis of a computer program (Maple) which

allows rapid solution of various sorting parameters (Hoyos et al., 2000). The program enables the simulation of numerous separations under varying flow conditions to obtain theoretical predictions of target cell recovery. Using this computer program, Hoyos et al. obtained reasonable agreement between predicted and experimental recoveries for separations of magnet-doped, micrometer-sized particles with an experimentally determined distribution of magnetophoretic mobilities.

The concept of magnetophoretic mobility derives from an analogy with electrophoretic mobility. The magnetophoretic mobility of a cell, m , is defined as

$$m = v_c / S_m \quad (1)$$

where v_c is the velocity of the cell in the magnetic field and S_m is the magnetic force field strength (the gradient of the magnetic energy density). The relationship among the magnetophoretic mobility, degree of magnetization (number of magnetic nanoparticles bound to the cell), and diameter of the cell was formulated previously by assuming that the forces acting on an immunomagnetically labeled cell are balanced (Chalmers et al., 1999a,b; McCloskey et al., 2000). Summarizing, the magnetophoretic mobility of a cell is given by

$$m = \frac{(\Delta\chi) V_m}{3\pi D_c \eta} \beta(ABC) \quad (2)$$

where $\Delta\chi$ is the difference in magnetic susceptibility between the magnetic bead and the suspending medium, V_m is the volume of the magnetic bead, D_c is the diameter of the cell, η is the viscosity of the suspension fluid, β is the number of magnetic beads bound to each primary antibody on a cell, and ABC is the antibody binding capacity of the cell. Immunomagnetically labeled cells can potentially bind large numbers of antibody-magnetic bead complexes ranging from hundreds to hundreds of thousands depending on the expression level of the target surface marker and the size of the paramagnetic nanoparticles and cells. This could result in a wide range of magnetophoretic mobilities for heterogeneous cell populations.

We have developed an analytical instrument for the experimental measurement of the magnetophoretic mobility distribution of a sample on a cell-by-cell basis (Chalmers et al., 1999a,b). This analytical instrument, referred to as cell tracking velocimetry (CTV), consists of a computer algorithm for particle tracking velocimetry and a well-designed magnetic device. In CTV analysis, immunomagnetically labeled cells are subjected to a constant magnetic energy gradient that results in a constant cell velocity in the direction of this gradient. Images of the moving cells are acquired by a CCD camera mounted on a microscope. Once digitized, the images are analyzed by the CTV programs to calculate the magnetophoretic mobility of each cell.

The work presented in this paper is intended to further test the QMS theory by using a well-characterized, heterogeneous biological system. Breast cancer cells (HCC1954) were used as the target cells to be separated by the QMS. Magnetophoretic mobility distributions of immunomagnetically labeled HCC1954 cells were determined using the CTV technique. HCC1954 cells labeled for the HER-2/neu antigen were mixed with unlabeled peripheral blood leukocytes (PBLs) to form a "spiked" sample for separation by the QMS. The fractional recoveries of the cells in QMS separations for different flow

parameters were examined and compared with theoretical predictions.

Materials and Methods

Preparation of the Cells. A breast carcinoma cell line overexpressing the HER-2/neu antigen (HCC1954) was used as the model for human cancer cells circulating in peripheral blood (Gardar et al., 1998). HCC1954 cells were obtained from the American Type Culture Collection (ATCC no. CRL-2338) and were cultured using an ATCC 30-2001 medium containing 10% fetal bovine serum (Sigma) in a T-75 flask, and were incubated at 37 °C in 5% CO₂.

Source leukocytes (buffy coat) were obtained from the American Red Cross before each day of experiments to serve as a source of PBL cells. Ficoll-Hypaque density gradient centrifugation (density 1.077 g/cm³) was used to separate mononuclear cells from the remaining plasma layer. Mononuclear cells were suspended in 5 mL of phosphate-buffered saline (PBS) containing 2 mM EDTA and 0.5% bovine serum albumin (BSA) (ORTHO, New Jersey) (hereafter referred to as PBS buffer). The cells were washed and suspended in PBS buffer to obtain the final PBL mixture.

If contaminated red blood cells were observed, they were removed by the addition of 25 mL of lysis buffer (154 mM NH₄Cl, 10 mM KHCO₃, 0.1 mM EDTA), followed by a 5 min incubation at room temperature. To investigate the potentially harmful effect of this lysis buffer on leukocytes, the cell size distribution was examined for different incubation periods. A decrease in the leukocyte cell size was observed for cell samples incubated at 15 min but not at 5 min. In addition, no cell clumping after 5 min of treatment was observed (visual observations). Finally, nonspecific binding studies using the secondary MACS antibody and leukocytes, either treated or untreated with lysis buffer, demonstrated no statistically detectable nonspecific binding. After treatment, the cells were washed and suspended in PBS buffer to obtain the final PBL mixture.

A two-step antibody process was used to label HCC1954 cells specific for the HER-2/neu antigen. A 30 µL sample of the primary antibody, mouse anti-HER-2/neu FITC (catalog no. 340553, Beckton Dickinson Immunocytometry Systems, San Jose, CA), was added per 10⁶ HCC1954 cells suspended in PBS buffer. The amount of primary antibody chosen was determined by a saturated fluorescence intensity value as determined by flow cytometry. The antibody/cell mixture was then incubated at 4 °C for 30 min, washed in 15 mL of buffer, and centrifuged at 500g for 7 min. Finally, the cell sample was resuspended in 20 µL of buffer per 1 million cells in preparation for the secondary antibody labeling.

Two different amounts of secondary antibody, mouse anti-FITC-MACS (catalog no. 487-01, Miltenyi Biotech), were used (Table 1). The incubation conditions were identical to those used in the primary labeling steps. Samples labeled with 8 µL of secondary antibody per 1 million cells were used for QMS separations.

PBL cells were labeled in preparation for flow cytometry analysis using mouse anti-CD45 PE antibodies (catalog no. IM2078, Immunotech, Paris, France). A 40 µL sample of the antibody was added per 10⁶ cells as recommended by the manufacturer.

Analysis of the Positive Fraction in a Cell Suspension. Analysis by Flow Cytometry. To assess QMS performance, it was necessary to accurately quantify the ratio of HCC1954 cells to PBL cells in various

Table 1. Magnetophoretic Mobility Data of Immunomagnetically Labeled HCC1954 Cells^a

amt of P* (µL/10 ⁶ cells)	amt of S* (µL/10 ⁶ cells)	N (cells)	mobility mean [mm ³ /(T A s)]	mobility SD [mm ³ /(T A s)]	mobility ^b CV (%)
0	0	205	-1.21E-06	3.17E-05	2607
0	0	572	-1.83E-06	1.84E-05	1006
0	0	322	-2.22E-06	6.34E-05	2857
0	0	698	-2.25E-06	3.14E-05	1391
0	0	1000	-4.51E-06	1.75E-05	388
0	0	559	-2.41E-06	3.25E-05	1650
0	1	357	-1.12E-05	6.41E-05	572
0	10	1014	-2.33E-06	5.78E-05	2480
0	100	742	9.13E-06	2.39E-05	262
30	4	275	1.58E-04	2.70E-04	171
30	4	430	5.25E-05	4.85E-05	92
30	4	429	1.89E-04	1.51E-04	80
30	4	1071	1.22E-04	1.62E-04	133
30	4	715	7.49E-05	5.76E-05	77
30	4	584	1.19E-04	1.38E-04	111
30	8	1089	3.31E-04	1.64E-04	49
30	8	936	1.73E-04	2.03E-04	117
30	8	881	4.83E-04	2.51E-04	52
30	8	829	3.84E-04	1.82E-04	47
30	8	1116	2.36E-04	2.38E-04	101
30	8	1078	2.96E-04	2.38E-04	80
30	8	764	2.60E-04	1.97E-04	76
30	8	956	3.09E-04	2.10E-04	75

^a P* = primary antibody. S* = secondary antibody. ^b CV = [SD·100/mean mobility].

cell suspensions. We considered two methods for determining this ratio: flow cytometry analysis and particle size counting.

Flow cytometry studies were performed on a Beckman-Coulter EPICS Elite II flow cytometer (Beckman-Coulter Corp., Miami, FL) equipped with a 488 nm, 15 mW air-cooled argon laser. Optical laser alignment calibration of the flow cytometer was performed using Beckman-Coulter's flow-check alignment fluorosphere beads (Beckman-Coulter) with coefficients of variation (CVs) that were routinely less than 2%.

Analysis of forward scatter and side scatter data was used to distinguish HCC1954 and PBL cells from red cells and platelets. The circled region in Figure 2A indicates the gate set for HCC1954 cells (1) and PBL cells (monocytes (2), lymphocytes (3), and granulocytes (4)). Using this gating condition, red blood cells (5) and platelets (not shown) were excluded from the FITC-PE antibody analysis.

The cells selected by the gate determination shown in Figure 2A were then further analyzed using FITC versus PE 2-D analysis in the logarithmic mode. FITC and PE fluorescent light emissions were reflected through 550 nm (FITC) and 600 nm (PE) dichromic long-pass filters and collected through band-pass filters of 525 nm (FITC) and 575 nm (PE). Figure 2B shows a diagram of the four regions (R₁, R₂, R₃, and R₄) used to analyze the fluorescence data. An unlabeled mixture of HCC1954 and PBL cells was analyzed to determine autofluorescence/background levels (Figure 2C). The gates for FITC-positive cells and for PE-positive cells (shown as a vertical line and a horizontal line, respectively, on PE log vs FITC log plots) were set on the basis of these autofluorescence levels. Cells counted in R₁ were considered to be FITC-negative and PE-positive (F⁻/P⁺). Cells counted in R₂, R₃, and R₄ were considered to be F⁺/P⁺, F⁻/P⁻, and F⁺/P⁻.

Possible cross-binding of antibodies (anti-HCC1954 FITC to PBL cells and CD45 PE to HCC1954 cells) was investigated by flow cytometry analysis and fluorescence microscopy. A sample of PBL cells was labeled with both anti-HCC1954 FITC and CD45 PE antibodies and ana-

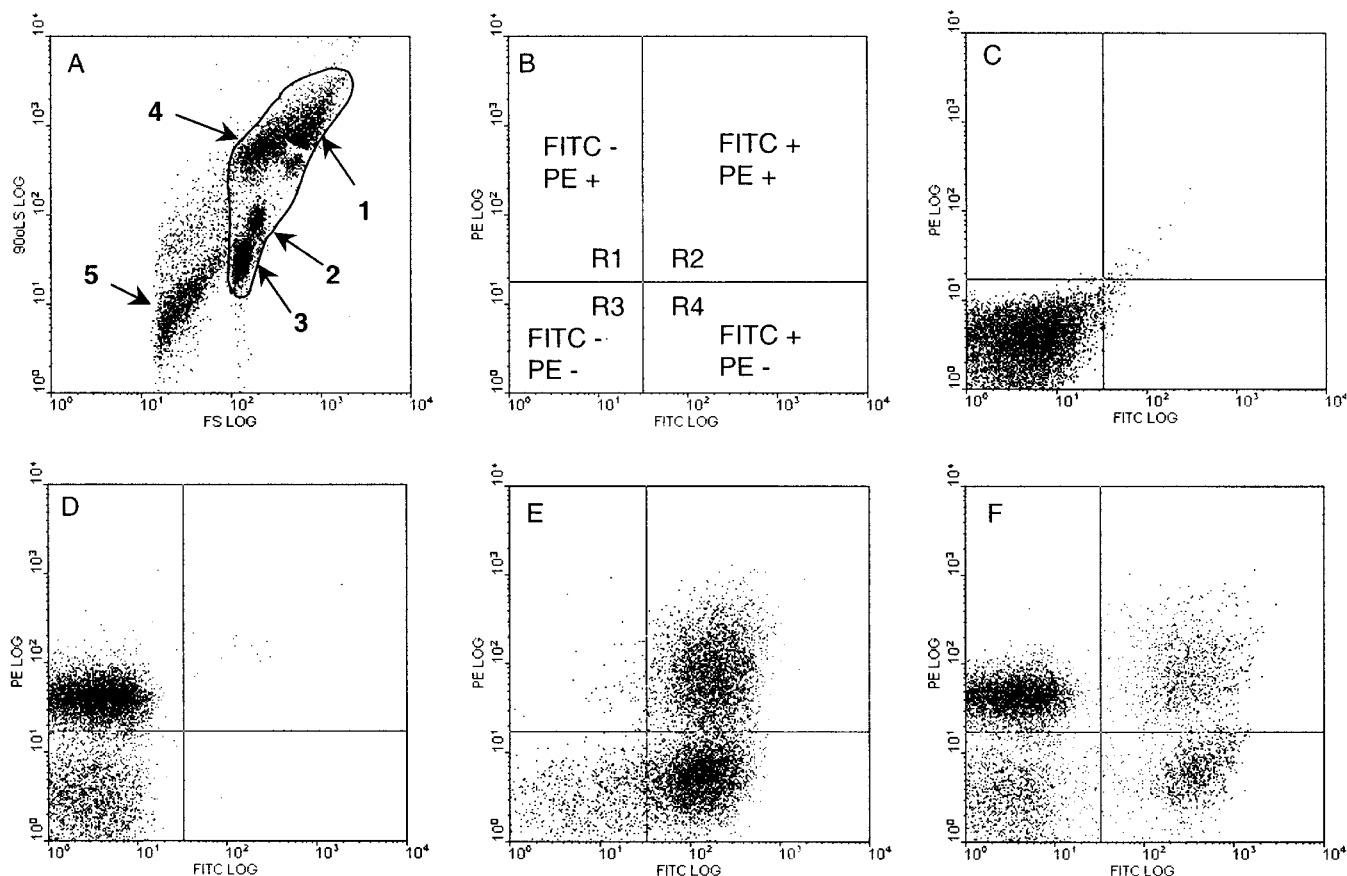


Figure 2. Flow cytometry analysis of the cell mixture of HCC1954 and PBL. (A) Dotplot of side scatter (90° light scatter) vs forward scatter on the logarithmic scale. The numbers represent the population of particular cell types: (1) HCC1954 cells, (2) monocytes, (3) lymphocytes, (4) granulocytes, and (5) red blood cells. The circled region indicates the range for FITC-PE analysis. (B) A diagram of the four regions (R_1 , R_2 , R_3 , and R_4) used to analyze fluorescence data in FITC-PE analysis. The gates for FITC-positive and for PE-positive (shown as a vertical line and a horizontal line, respectively) were set on the basis of the autofluorescent levels of unlabeled cells. R_1 = the region for FITC-negative and PE-positive (F^-/P^+), $R_2 = F^+/P^+$, $R_3 = F^-/P^-$, and $R_4 = F^+/P^-$. (C) FITC-PE analysis of the unlabeled cell mixture of PBL and HCC1954 cells (1:1). (D) Labeled PBL cells. (E) Labeled HCC1954 cells. (F) Labeled mixture of PBL and HCC1954 cells (1:1).

lyzed by flow cytometry (Figure 2D). The absence of cells in R_2 indicated that the anti-HCC1954 FITC antibody did not nonspecifically bind to the PBL cells. This result was confirmed by fluorescence microscopy, which showed PBL cells emitting only PE (red) signals (image not shown). A sample of HCC1954 cells was then labeled with both anti-HER-2/neu FITC and CD45 PE antibodies and analyzed by flow cytometry (Figure 2E). The presence of about half of the analyzed HCC1954 cells in R_2 indicated that a significantly high level of cross-binding between CD45 PE antibodies and HCC1954 cells had occurred. Fluorescence microscopy confirmed the flow cytometry results.

As a consequence of the nonspecific binding of the CD45 PE antibody to the HCC1954 cells, it was determined that, for a spiked sample, cells in R_2 and R_4 were counted as HCC1954 cells. Cells in R_1 were counted as PBLs, and cells in R_3 were considered to be cell debris. The formula to calculate the fraction of positive cells (HER-2/neu FITC) in a cell suspension of HCC1954 and PBL cells by flow cytometry analysis is consequently defined as

$$P_{HCC} = \frac{N_{R_2} + N_{R_4}}{N_{R_1} + N_{R_2} + N_{R_4}} \quad (3)$$

where P_{HCC} is the fraction of HCC1954 cells in the cell suspension, and N_{R_1} , N_{R_2} , and N_{R_4} are the number of cells

counted in R_1 , R_2 and R_4 , respectively. Figure 2F shows a typical result of flow cytometry analysis of a cell mixture that was labeled with both anti-HER-2/neu FITC and CD45 PE antibodies.

Cell Size and Number Analysis. A Coulter Multi-sizer II system (Beckman-Coulter) with a 100 μm aperture diameter was used to determine cell numbers and cell diameters. Cell suspensions to be analyzed were diluted in 10 mL of Isoton III electrolyte solution (Beckman-Coulter). Particle data were collected over a diameter range of 1.73–63.10 μm , subdivided into 256 bins.

A typical cell size distribution of a mixture of HCC1954 and PBL cells is shown in Figure 3. Peak A corresponds to lymphocytes, peak B to monocytes and granulocytes, and peak C to the HCC1954 cells. The clear difference in the cell size distribution between PBL and HCC1954 cells allowed us to define diameter ranges that would be used to determine the ratio of HCC1954 to PBL cells in a mixture. A background range was set at 1.73–5.92 μm , the diameter of PBL ranged from 5.92 to 12.57 μm , and the diameter of HCC1954 ranged from 12.57 to 30.07 μm . The small numbers of counts above 30.07 μm were disregarded. The formula to calculate the fraction of HCC1954 cells in a cell suspension by particle size analysis is thus defined as

$$P_{HCC} = \frac{N_{HCC}}{N_{HCC} + N_{PBL}} \quad (4)$$

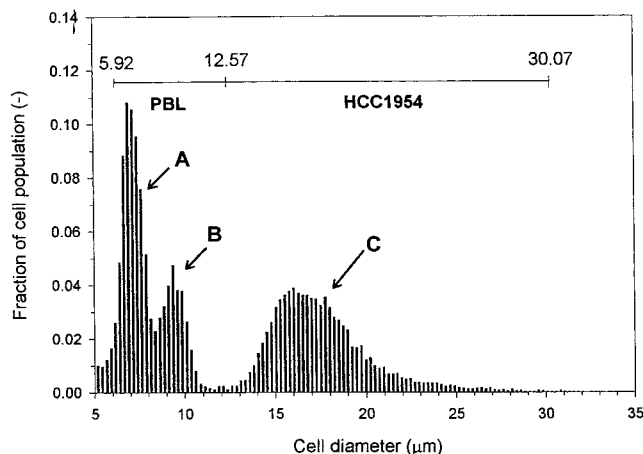


Figure 3. Cell size distribution of the cell mixture of HCC1954 and PBL measured by a particle size analyzer (Coulter Multi-sizer II). The distributions A, B, and C are for lymphocytes, a mixture of monocytes and granulocytes, and HCC1954 cells, respectively. The size ranges for PBL and HCC1954 were set from 5.92 to 12.57 μm for PBL and from 12.57 to 30.07 μm for HCC1954.

where N_{HCC} is the number of cell counts in the HCC1954 range and N_{PBL} is the number of cell counts in the PBL range.

Comparison of the HCC1954 Ratio Measured by Flow Cytometry and by the Particle Size Counter.

To compare the fraction positive data obtained by the two methods, HCC1954 and PBL cells were mixed in PBS buffer at different percentages, with a constant total cell concentration of 10^5 cells/mL. The fractions positive for HCC1954 cells for each of these samples were then measured by both the particle size and the 2-D flow cytometry analysis methods. Figure 4 shows reasonable agreement between these two methods within the range of interest. As a result of the rapid and inexpensive nature of sample analysis by particle size counting, and close agreement with the conventional flow cytometry technique, this method was chosen to measure the fraction of HCC1954 cells in the experimental samples.

CTV Analysis. The descriptions and use of the CTV technique have been previously presented (Chalmers et al., 1999a,b; Nakamura et al., 2000). No changes or modifications from these reports were used in this study.

Model Predictions of QMS Performance. The theoretical model of the QMS sorting process has been described elsewhere (Williams et al., 1999). The following assumptions were made: (1) pointlike cells, (2) no inter-cell interactions, (3) perfect field and flow geometry, (4) magnetic and viscous forces only, and (5) no fringing fields at the ends of the QMS unit. We have developed a computer algorithm that reads in a cell mobility histogram measured by CTV analysis and computes cell retrieval factors as a function of adjustable flow parameters (Q_a , Q_a/Q_t , and Q_a/Q_b) based on the geometry and magnetic field characteristics of a particular QMS system. The retrieval factors are defined as

$$F_i = N_i/N_f \quad (5)$$

where F_i is the retrieval factor in fraction i (either stream a or stream b), N_i is the number of cells collected in fraction i , and N_f is the number of cells fed to the separator. This algorithm was executed using a Maple V (Waterloo Maple, Inc., Ontario, Canada) worksheet run on an IBM-compatible PC. Additional details of the

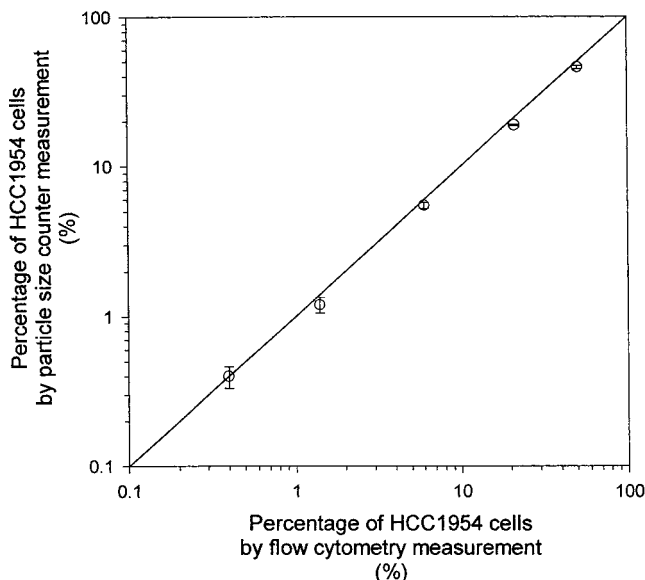


Figure 4. Comparison of two analytical methods to measure the purity of HCC1954 cells in the cell mixture. HCC1954 cells and PBL cells were mixed at different ratios at 10^5 cells as the total cells. The percentages of HCC1954 cells in the sample were measured both by flow cytometry analysis and by particle size counting.

algorithm for recovery calculation are given elsewhere (Hoyos et al., 2000).

QMS Setup and Operation. The design and materials of construction for the QMS channel and magnet system have been described elsewhere (Zborowski et al., 1999). Figure 1 presents an overview of the system. The quadrupole magnet used for these experiments had a maximum magnetic field strength (B_0) of 1.334 T and mean force field strength (S_m) of 2.382×10^8 (T A)/m². Important measurements for the QMS channel (QMS Mk. IV) used in this study were as follows: inner rod radius (r_i) 2.38 mm, outer tube inner radius (r_o) 4.41 mm, splitter radius (r_s) 3.22 mm. Table 2 summarizes these specifications.

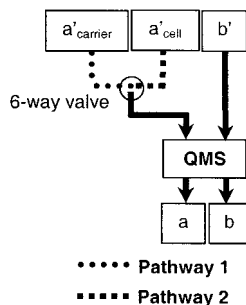
Two double-syringe pumps and one single-syringe pump (type 33 syringe pump, Harvard Instrument Inc., Massachusetts) were used to control the flow parameters. Teflon tubing with an internal diameter of 0.8 mm was used for fluid connections. The two fluid pathways used in these experiments are diagrammed in Figure 5. A six-way valve (Rheodyne 7751I, Alltech Associates, Inc., Illinois) was used to switch between these two fluid pathways during pump operation without disrupting fluid flow within the channel. Fluid pathway 1 was used to feed carrier from syringes a' and b' to the channel, while fluid pathway 2 was used to feed the cell sample from syringe a' and carrier from syringe b' . For both fluid pathways, eluted samples were collected in syringe a (depleted fraction) and syringe b (enriched fraction). Flow rate settings for each pump were governed by the relation

$$Q_{a'} + Q_{b'} = Q_a + Q_b \quad (6)$$

Prior to the actual separation, the system was filled with filtered, degassed PBS buffer. The outlet and cell feed syringes were then weighed and mounted. To establish steady-state flow before the cells entered the separator channel, the pumps for a' , b' , a , and b were started using fluid pathway 1. After a few seconds, the pump for a' was started and the six-way valve was

Table 2. QMS System Parameters

parameter	value
maximum field (B_0)	1.334 T
mean force field strength	2.38×10^8 (T A)/m ²
bore diameter (pole tip to pole tip)	9.07 mm
magnet length (QMS separation element length)	76.2 mm (3 in.)
inner rod radius (r_i)	2.38 mm
outer tub radius (r_o)	4.41 mm
splitter radius (r_s)	3.22 mm

**Figure 5.** Flow pathways of the QMS system.

switched to pathway 2 to allow cells to enter the channel. After the entire cell sample had been fed, the six-way valve was switched back to pathway 1 so that additional carrier solution could be fed through the a' inlet. This additional carrier solution was used so that cells that otherwise would have been retained in the flow channel would be eluted. After a volume of additional carrier approximately equal to 4 times the working volume of the QMS had been fed, the pumps were turned off and the outlet and cell feed syringes were weighed. The difference in the weight of these syringes before and after the separation was combined with PBL and HCC1954 cell count data to calculate the cell recovery and fraction positive.

Results

Magnetophoretic Mobility of HCC1954 Cells. As described in the Materials and Methods, HCC1954 cells were immunomagnetically labeled targeting the HER-2/neu antigen using a two-step labeling procedure. Flow cytometry analysis showed that 92.3% (SD of 4.64, $n = 6$) of the cells were counted in the positive FITC signal range (data not shown).

CTV analysis was used to determine the magnetophoretic mobility distribution of cell populations on different days and using different labeling conditions. Table 1 shows the labeling conditions and corresponding mean magnetophoretic mobility data. Unlabeled HCC1954 and PBL cells both had mean magnetophoretic mobilities near zero (-2.41×10^{-6} and -4.86×10^{-6} mm³/(T A s), respectively). Typical magnetophoretic mobility distributions of unlabeled cells are shown in Figure 6A,B. The data for HCC1954 cells labeled under two different conditions, 4 and 8 μ L of secondary antibody per 1 million cells, show mean magnetophoretic mobilities that were more than an order of magnitude greater than the mean mobilities of unlabeled cells (1.19×10^{-4} and 3.09×10^{-4} mm³/(T A s), respectively). Typical mobility distributions of labeled HCC1954 cells are shown in Figure 6A,B. Figure 6C shows the variation of the mean magnetophoretic mobility in different cell samples, which were labeled on different days. Vertical bars represent the standard deviation of the mean magnetophoretic mobility for each labeling condition.

Cell Separation by the QMS. Three adjustable QMS flow parameters are incorporated into the theoretical

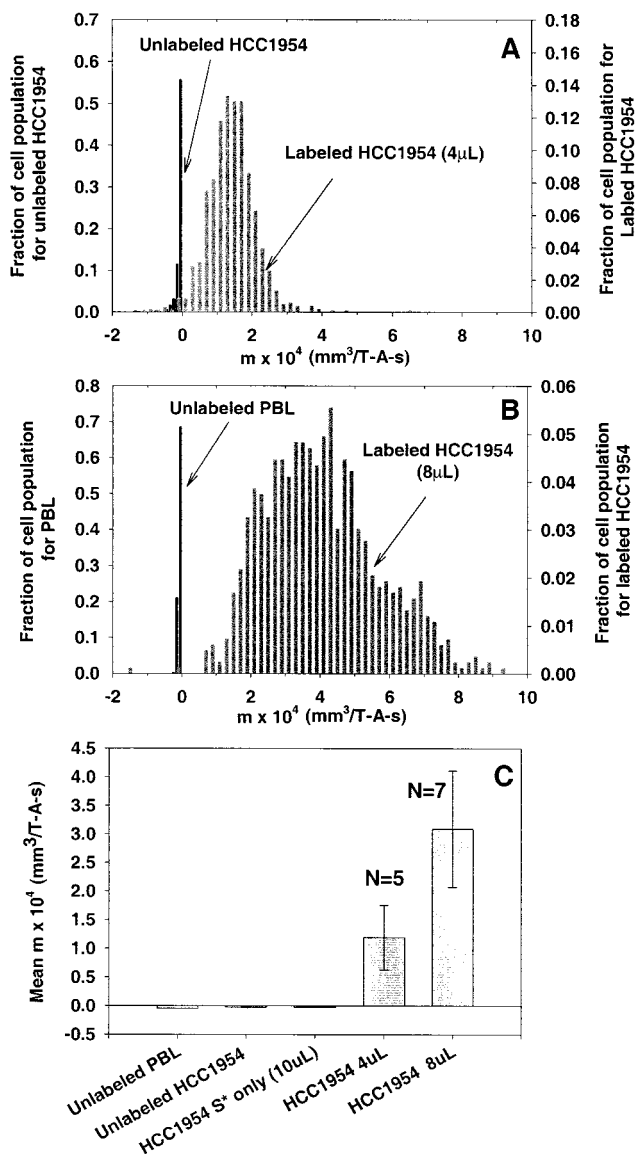


Figure 6. Magnetophoretic mobility of the HCC1954 cells: representative examples of the magnetophoretic mobility distribution of (A) unlabeled HCC1954 and labeled HCC1954 cells (4 μ L of primary antibody/10⁶ cells) and (B) unlabeled PBL and labeled HCC1954 cells (8 μ L of primary antibody/10⁶ cells), (C) mean magnetophoretic mobility with standard deviations of multiple measurement as error bars.

model of the sorting process: (1) total flow rate (Q_t), (2) inlet flow rate ratio (Q_a/Q_t), and (3) outlet flow rate ratio ($Q_{a'}/Q_t$). For a given system magnetic field strength and channel geometry, Q_t controls the time cells spend in the magnetic field region, and consequently controls the ratio of eluted to retained cells ($(F_a + F_b)/F_w$). To facilitate the following description, and assist in the interpretation of the data, Figure 7 has been included, which is an enlargement of the QMS in the region of the magnetic energy gradient (QMS separation element). The parameters Q_a/Q_t and $Q_{a'}/Q_t$ combine to control the minimum distance that cells must migrate to be collected in fraction b. In the theoretical model of the sorting process, the inlet flow rate ratio (Q_a/Q_t) and the outlet flow rate ratio ($Q_{a'}/Q_t$) determine the positions of imaginary fluid stream boundaries, the inner splitting cylinder (at $r = r_{ISC}$) and the outer splitting cylinder (at $r = r_{OSC}$), respectively. Feed cells are assumed to distribute evenly between the inner wall of the channel (at $r = r_i$) and the inner splitting cylinder. At the fluid outlet, cells that have a radial

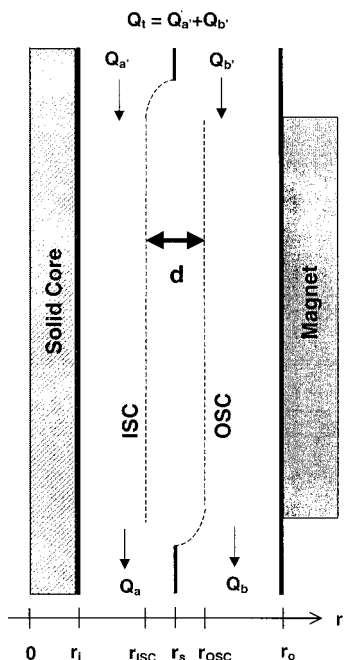


Figure 7. Concept of transport lamina thickness (d) in the QMS. Two imaginary boundaries of flows for the inlet (a' and b') and for the outlet (a and b) were considered the inner inlet splitting cylinder (ISC) and outlet splitting cylinder (OSC), respectively. The positions of both the ISC and OSC were calculated on the basis of the flow rates of the inlets and outlets and the annular velocity profile of the flow in the QMS (Williams et al., 1999; Hoyos et al., 2000). The transport lamina thickness (d) was defined as the distance between the ISC and OSC. The transport lamina thickness was the minimum distance that cells needed to travel to be collected in the b fraction (enriched fraction).

position between r_{OSC} and r_0 will be collected in fraction b. On the basis of the model, a minimum distance that cells must travel to be collected in the b stream, termed the transport lamina thickness (d) can be defined as

$$d = r_{OSC} - r_{ISC} \quad (7)$$

The previously published work of Hoyos et al. (2000) demonstrated that reasonable agreement between model simulations and experimental results can be obtained for an optimized total flow rate (Q_t). The study by Hoyos et al. (2000) used a homogeneous sample of magnetically doped particles in which the magnetophoretic mobility had been experimentally measured. On the basis of this agreement between the model simulations and experimental data, the optimum Q_t for this study was obtained using the same type of model simulations and the experimentally determined magnetophoretic mobility of the immunomagnetically labeled HCC1954 cells. Since the magnetophoretic mobility of the immunomagnetically labeled HCC1954 cells was determined before each set of experiments, model simulations were performed prior to each set of experiments. However, as can be observed from Table 3, the value of Q_t only changed for one set of experiments. The effect of the transport lamina thickness was studied by holding Q_a/Q_t constant at 0.1 and varying Q_a/Q_t from 0.1 to 0.4, with a corresponding variation of d from 0 to 491 μm . A total of 25 magnetic cell separations were performed.

The conditions used for separations performed with magnetically labeled, unmixed HCC1954 cells (sample A) are shown in Table 3. At a total flow rate of 12–20 mL/min, the flow is well within the laminar flow region

and cell damage, as a result of any hydrodynamic forces, would not be expected. This theoretical observation was supported by experimental results which indicated that the cell size distribution of both PBL and HCC1954 cells remained the same before and after QMS separation. Also, visual inspection of the fluid collected from the separator did not indicate any observable cell debris. Consequently, it is highly unlikely that false measurements of cell counts could result from cell destruction or damage to the larger HCC1954 cells in such a way that they would be mistakenly counted as smaller PBL cells.

The recoveries of HCC1954 cells in fraction a ($F_{a,HCC}$) and in fraction b ($F_{b,HCC}$) were measured for different values of d (Figure 8). When d was 0, $F_{a,HCC}$ and $F_{b,HCC}$ were approximately 0.2 and 0.7, respectively. As d increased, $F_{a,HCC}$ gradually increased and $F_{b,HCC}$ decreased. This trend closely matched theoretical predictions calculated on the basis of the magnetophoretic mobility of HCC1954 cells, Figure 6b. A comparison of experimental and theoretical values of $F_{a,HCC}$ and $F_{b,HCC}$ for different values of d is also presented in Figure 8.

The conditions used for experiments performed with mixtures of 1% labeled HCC1954 cells and 99% unlabeled PBL cells ($P_{a,HCC} \approx 0.01$; samples B, C, and D) are also shown in Table 3. In addition to the determination of $F_{a,HCC}$ and $F_{b,HCC}$, $F_{a,PBL}$ and $F_{b,PBL}$ were also measured. Figure 9 shows the results of separations using sample B. Figure 9A presents $F_{a,HCC}$ and $F_{b,HCC}$ as functions of d . Consistent with the behavior of unmixed HCC1954 cells, as d increased $F_{a,HCC}$ increased and $F_{b,HCC}$ decreased. Figure 9B shows the recovery of PBL cells (unlabeled) in fractions a and b. $F_{b,PBL}$ was approximately 0.15 at $d = 0$ and decreased as d increased. Theoretically, all PBL cells should have been collected in fraction a, regardless of d due to their negative mobility values. Figure 9C presents the fraction of HCC1954 cells in fractions a and b ($P_{a,HCC}$ and $P_{b,HCC}$) also as a function of d . As d increased, $P_{b,HCC}$ increased up to 0.5. The results of cell separations using samples C and D showed similar relationships between d and the cell recoveries.

Discussion

Flow cytometry analysis of six samples of HCC1954 cells labeled with the primary antibody specific for the HER-2/neu antigen indicated that, on average, 92.3% of the cells were positive. Saturation studies (data not shown) suggest that higher percent positive cell suspensions, as determined by flow cytometry, could not be obtained by adding more primary antibody. The most probable explanation for the failure to achieve 100% purity could be the heterogeneity of the target antigen (HER-2/neu) expression level in the HCC1954 cell population. Some cells may express HCC1954 protein at a sufficiently lower level so that their FITC signals were too weak to be considered as positive. However, it does not necessarily mean that there was no HER-2/neu antigen for these cells counted as negative. Since we immunomagnetically labeled HCC1954 cells with secondary antibody–magnetic beads complex, even the low expression of HER-2/neu antigen might be high enough as a driving force for magnetic cell separation.

The goal of the secondary labeling step was to impart the HCC1954 cells with a sufficient degree of magnetophoretic mobility for QMS separation. Theoretical predictions of the performance of the QMS system (Williams et al., 1999) indicate that the throughput is directly proportional to the mobility of immunomagnetically labeled cells. Theoretical prediction and the experimental results of labeled HCC1954 cells both demonstrate that

Table 3. QMS Separation of the Mixture of HCC1954 and PBL Cells

expt	flow conditions			cell feed		C_{HCC} (cells/mL)	$P_{HCC,a}$	throughput (cells/s)	highest $F_{b,HCC}$	highest $P_{HCC,b}$
	Q_t (mL/min)	Q_a/Q_t	Q_b/Q_t	V (mL)	C_t (cells/mL)					
A	20	0.1	0.1–0.4	2	1.19E+05	1.2E+05	1	3.95E+03	0.691	n/a
B	20	0.1	0.1–0.3	2	9.88E+06	1.2E+05	0.012	3.29E+05	0.890	0.480
C	12	0.1	0.1–0.4	1.5	9.18E+06	1.2E+05	0.014	1.84E+05	0.663	0.483
D	20	0.1	0.1–0.4	2	9.41E+06	1.2E+05	0.012	3.14E+05	0.767	0.472

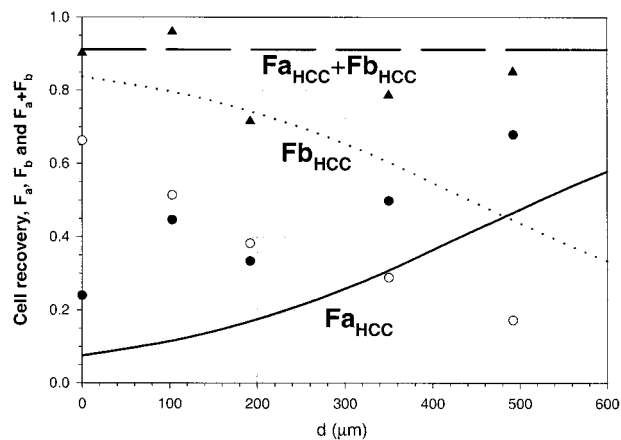
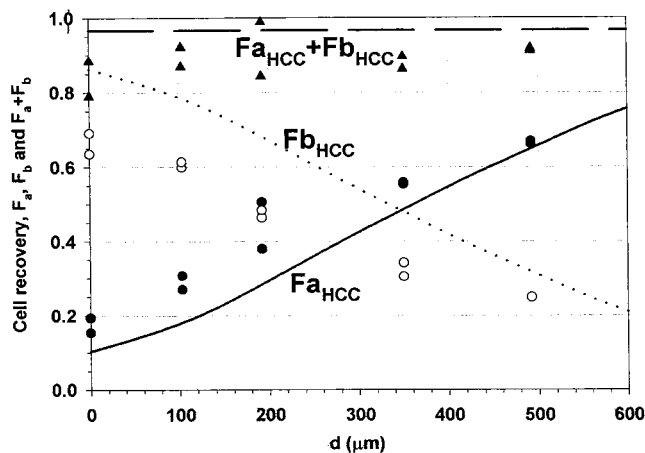


Figure 8. Recovery of labeled HCC1954 cells in the outlet fractions by QMS sorting. The experimental results of $F_{a,HCC}$ (closed circles), $F_{b,HCC}$ (open circles), and total recovery $F_{a+b,HCC}$ ($=F_{a,HCC} + F_{b,HCC}$) (closed triangles) and the theoretical prediction of $F_{a,HCC}$ (continuous line), $F_{b,HCC}$ (dotted line), and $F_{a+b,HCC}$ (dashed line) were plotted on the basis of the transport lamina thickness (d).

the achieved mobility level (shown in Table 1) was high enough to yield a significant recovery of target cells in the b fraction at high throughput (3.4×10^5 cells/s) using the QMS system. Ongoing optimization studies in our laboratory also indicate that average mobilities as high as $1 \times 10^{-3} \text{ mm}^3/(\text{T A s})$ can be achieved using much higher concentrations of secondary antibody. Such a mobility value is approximately 10 times higher than was used in this study, though the amount of antibodies required for such high mobilities is impracticably large (more than $100 \mu\text{L}$ of secondary antibody/ 10^6 cells).

In the experiments presented in this paper, the behaviors of immunomagnetically labeled HCC1954 cells were examined using both pure and mixed samples. Although a reasonable match between simulated and experimental recovery was seen, the predicted recovery of the immunomagnetically labeled HCC1954 cells in the b stream ($F_{b,HCC}$) was consistently overestimated and the predicted recovery in the a stream ($F_{a,HCC}$) was consistently underestimated, relative to the experimental results. In addition, the distribution of unlabeled cells in the two exit streams was suboptimal. Theoretical simulations predict that no unlabeled cells should appear in the b stream, $F_{b,PBL} = 0$. While $F_{b,PBL}$ did decrease as d was increased (Figure 9b), values of $F_{b,PBL}$ as high as 0.15 were observed when $d = 0$. This phenomenon is referred to as cell crossover.

It is proposed that these two suboptimal performance observations, lower values of $F_{b,HCC}$ relative to theoretical simulations and nonzero values of $F_{b,PBL}$, are independent effects that might or might not have the same cause. There are several reasons for this hypothesis. First, comparisons of experimental values of $F_{b,HCC}$ in Figure 8 (100% HCC1954 cells in the feed, $F_{a,HCC} = 1.0$) and Figure 9A (1% HCC1954 cells in the feed, $F_{a,HCC} = 0.1$) are very similar, indicating that the presence of PBL cells did not

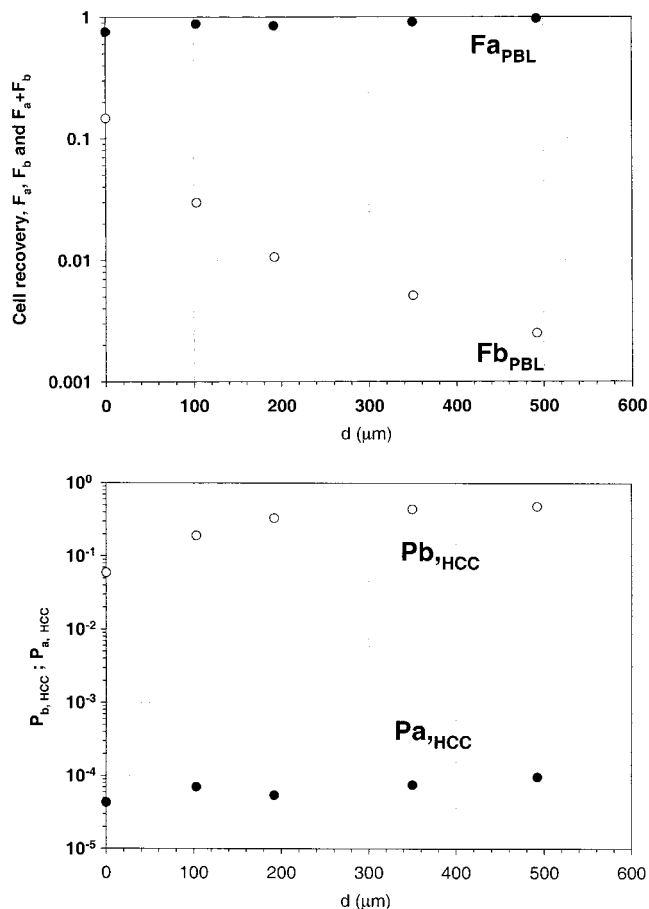


Figure 9. Performance of the QMS on the cell mixture at different thicknesses of the transport lamina: (A, top) recovery of HCC1954 cells in the outlet fractions, (B, middle) recovery of PBL cells in the outlet fractions, (C, bottom) ratio of HCC1954 cells in the outlet fractions. The values of fraction a (closed circles) and fraction b (open circles) were plotted on the basis of the transport lamina thickness (d). The total recovery of HCC1954 cells (closed triangles) was also plotted in (A).

cause the decrease in $F_{b,HCC}$. Second, Hoyos et al. (2000) also reported experimental values of F_b for 100% mag-

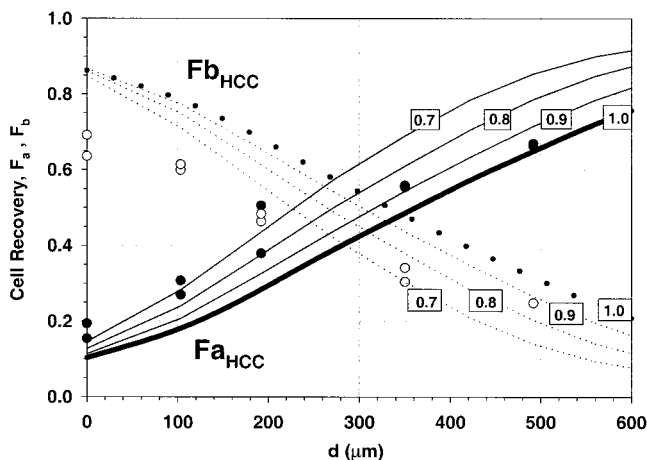


Figure 10. A copy of Figure 8 with additional theoretical predictions using 0.9, 0.8, and 0.7 of the experimentally determined magnetophoretic mobilities of the HCC1954 cells.

netically doped microspheres lower than the theoretical simulations predicted. Third, studies (not shown) with nonmagnetically labeled PBL cells and Chinese hamster ovary cells have shown cell crossover which decreased with increasing transport lamina thickness (d). The level of crossover in each unlabeled cell type was quite similar to that in the spiked cell mixture at a given transport lamina thickness. Thus, we concluded that crossover was related to the cell motion due to the hydrodynamic force/flow in the QMS column rather than the magnetic behavior of the cells in the magnetic field. Computer simulations of the hydrodynamic flow in the QMS indicate that small imperfections in the location of the flow splitter (Figure 1) can have a significant, negative impact on cell crossover. Ongoing experimental studies using distorted flow splitters confirm these computer simulations. These and other studies have led to improved QMS columns which are currently under development.

There are a number of hypotheses for the suboptimal values of $F_{b,HCC}$. One explanation is that the experimentally determined magnetophoretic mobilities from the histograms of the immunomagnetically labeled HCC1954 cells (i.e., Figure 6A) overestimate the true values. The computer simulations used to predict the performance of the QMS were based on the magnetophoretic mobility data. However, Moore et al. (2000) experimentally demonstrated that the CTV system reasonably measures the mean magnetophoretic mobility of magnetically doped microspheres when compared to measurements of the same microspheres using a vibrating sample magnetometer (VSM). In addition, Hoyos et al. (2000) demonstrated that while the experimentally determined values of F_b were consistently below the computer simulation predictions, the optimum total flow (Q_t) was accurately predicted. Q_t determines, among other things, the residence time that a cell or microsphere spends in the magnetic field. Consequently, experimental overprediction of the mean magnetophoretic mobility would result in a lack of agreement between the simulated and experimentally determined, optimal Q_t .

A final argument against the idea that the experimentally determined values of the magnetophoretic mobility of a labeled cell population overestimate the actual values is presented in Figure 10. In this figure, the experimental data (solid and open circles) and computer-simulated values (bold solid and dotted lines) from Figure 8 are presented as well as computer-simulated values using

experimental magnetophoretic mobility values that are 90%, 80%, and 70% of the actual values. As can be observed, the decrease in mobility values does not improve the fit between the model and experimental results. While the above arguments indicate that mean values of magnetophoretic mobility are correct, it is possible that the distribution is incorrect. Further investigation of this hypothesis is ongoing.

Hoyos et al. (2000) hypothesized about the suboptimal agreement between theoretical predictions and experimental recoveries in their studies on magnetically doped microspheres. The focus of their discussion was on the effects of unmodeled secondary flow. It is very possible that such flows could explain both the lack of agreement of $F_{b,HCC}$ and $F_{a,HCC}$ with the simulations and cell crossover.

Conclusion

In these experiments, the behavior of labeled and unlabeled cells in the QMS was studied. High-throughput separations were performed, with high recoveries of target cells in an enriched fraction. A reasonable match between experimental recoveries and theoretical predictions was observed. In addition, these experiments suggest the way in which the theoretical model of the sorting process can be combined with CTV mobility data, magnetic labeling studies, variation of flow parameters, and separator design modifications to facilitate rational optimization of the QMS cell separation process. An improved QMS design is currently under development which will theoretically both increase cell throughput and decrease unlabeled cell crossover.

Notation

ABC	antibody binding capacity
C	cell concentration
CTV	cell tracking velocimetry
d	transport lamina thickness
$F_{x,y}$	fractional recovery of the "y" cells in flow stream "x" relative to the total amount of "y" cells fed
m	magnetophoretic mobility
N_i	number of cells in the "i" stream
$P_{x,y}$	fraction of the "y" cells in the "x" flow stream
Q_t	total flow rate
$Q_{a'}$	inlet flow rate (cell sample)
$Q_{b'}$	inlet flow rate (carrier fluid)
Q_a	outlet flow rate (depleted fraction)
Q_b	outlet flow rate (enriched fraction)
QMS	quadrupole magnetic cell sorter
r	radial coordination
R_1, R_2, R_3, R_4	regions in the FITC-PE flow cytometry analysis
S_m	magnetic force field strength (a gradient of the magnetic energy density)
V	volume
V_m	volume of a magnetic bead
r	reduced radius ($= r/r_0$)

Subscripts

a	QMS outlet port designation
b	QMS outlet port designation
a'	QMS inlet port designation
b'	QMS inlet port designation
ISC	inlet splitting cylinder
OSC	outlet splitting cylinder
t	total

Acknowledgment

This study was supported by grants from the NCI (R01 CA62349 to M.Z., R33 CA81662-01 to J.J.C., and CA16058-25 to The Ohio State University) and the NSF (BES-9731059). We thank Mr. Andy Oberyszyn at The Ohio State University Analytical Cytometry Laboratory for performing the FACS analysis and making technical suggestions, and Mr. John (Pete) Gosser at the physics machine shop at The Ohio State University for expert technical help in machining parts of the QMS.

Appendix

1. QMS Theory. We have constructed a theory of the magnetic sorting process in the QMS (QMS theory) (Williams et al., 1999). The theory is based on (1) the magnetophoretic mobility distribution of the cell sample, (2) the annular flow geometry of the QMS, (3) the magnetic field strength, and (4) the adjustable flow conditions of the QMS that govern sample fractionation. Summarizing, the quadrupole magnetic field strength, S_m , in the QMS is given by

$$S_m = \frac{B_0^2}{\mu_0 r_0^2} \quad (8)$$

where B_0 is the magnetic field intensity at the inner surface of the outer wall, r_0 is the radius of this inner surface, and $\rho = r/r_0$ (r being the radial distance from the annular axis).

The QMS has two fluid inlets, a' and b' , and two fluid outlets, a and b (Figures 1 and 7). Generally, the inlets and outlets are used as follows: a' for the cell sample, b' for the carrier fluid, a for the depleted fraction, and b for the enriched fraction. In the operation of the QMS, the inlet and outlet flow rates can be changed according to the relation

$$Q_t = Q_{a'} + Q_{b'} = Q_a + Q_b \quad (9)$$

where Q_t is the total flow rate and $Q_{a'}$, $Q_{b'}$, Q_a , and Q_b are the flow rates of a' , b' , a , and b , respectively.

The laminar flow velocity profile in an annular channel is given by

$$v(\rho) = 2 \left(\frac{\langle v \rangle}{A_1} \right) (1 - \rho^2 - A_2 \ln \rho) \quad (10)$$

where $\langle v \rangle$ is the mean flow velocity and A_1 and A_2 are constants that depend on the geometry of the coaxial cylinders in the QMS. The mean flow velocity $\langle v \rangle$ is calculated from the equation

$$Q = \langle v \rangle \pi r_0^2 (1 - \rho_1^2) \quad (11)$$

where $\rho_1 = r_1/r_0$ (r_1 being the radius of the inner rod). We consider an imaginary boundary of inlet flow streams (inlet splitting cylinder, ISC) which separates the flow from inlet a' and the flow from inlet b' (Figure 7). Cells fed to the QMS from inlet a' are assumed to locate between r_1 and r_{ISC} before being exposed to the magnetic field. An analogous boundary can be considered between the outlet flow streams (outer splitting cylinder, OSC). We consider three trajectories that result in different outcomes for sorted cells. Cells with a final position between r_1 and r_{OSC} are collected in fraction a. Cells between r_{OSC} and r_0 are collected in fraction b. Cells that reach the wall are retained inside the separator as

fraction w. The relative positions of the ISC (ρ_{ISC}) and OSC (ρ_{OSC}) were obtained numerically by solving the integral equations

$$Q_{a'} = \frac{4\pi r_0^2 \langle v \rangle}{A_1} \int_{\rho_1}^{\rho_{ISC}} (1 - \rho^2 - A_2 \ln \rho) \rho \, d\rho \quad (12)$$

$$Q_a = \frac{4\pi r_0^2 \langle v \rangle}{A_1} \int_{\rho_1}^{\rho_{OSC}} (1 - \rho^2 - A_2 \ln \rho) \rho \, d\rho \quad (13)$$

After the positions of the ISC and the OSC were obtained, the transport lamina thickness (d) was calculated by

$$d = r_{OSC} - r_{ISC} \quad (14)$$

This thickness (d) was the minimum distance that cells needed to travel to be collected in fraction b.

The trajectory of a cell was determined by solving the integral

$$\int_0^z dz = \int_{\rho_1}^{\rho} \frac{v(\rho)}{u_m(\rho)} r_0 \, d\rho = \frac{2\langle v \rangle r_0}{A_1} \int_{\rho_1}^{\rho} \frac{(1 - \rho^2 - A_2 \ln \rho)}{m S_m} \, d\rho \quad (15)$$

where u_m is the magnetically induced radial velocity. The axial length of the force field (L) was assumed to be equal to the length of the magnet. Additional details of the QMS theory are given elsewhere (Williams et al., 1999; Zborowski et al., 1999).

2. Algorithm for the Theoretical Recovery Calculation. The magnetophoretic mobility of each cell in a cell sample was individually measured by the CTV technique. Typically, several hundred cells were analyzed. The obtained magnetophoretic mobility data were further sorted to create a histogram as paired mobility–frequency increment data (as shown in Figure 6). Typically, logarithmic fractions with 20 bins per order of magnitude were used for the histogram.

A computer algorithm was developed to calculate a large number of cell trajectories over a number of initial cell positions with a given magnetophoretic mobility distribution of the cell population. The theoretical recovery as a function of the flow parameters was calculated with a Maple V (Waterloo Maple, Ontario, Canada) computer program run on an IBM-compatible personal computer. The program read in paired mobility–frequency increment data obtained from the CTV analysis. From each data set's mobility value, two trajectories were assigned: one beginning at $r = r_1$ and the other beginning at $r = r_{ISC}$ when the cells are subjected to a magnetic field in the QMS column. The terminal radii at the end of the magnetic field were determined by calculating the cell trajectories. A series of conditional statements enabled the calculation of the single data pair's fractional recoveries at outlet a or b or the wall, w. These recoveries were calculated using external subroutines. Each recovery was then weighted by the corresponding mobility frequency. The process was repeated for all the data pairs, while the weighed recoveries were summed, yielding the overall recoveries in outlets a and b and w, for the choice of experimental conditions including the total flow rate (Q) and the flow ratios of the inlet ($Q_{a'}/Q$) and outlet (Q_a/Q). Additional details of the algorithm are given elsewhere (Hoyos et al., 2000).

References and Notes

- (1) Bilkenroth, U.; Taubert, H.; Riemann, D.; Rebmann, U.; Heynemann, H.; Meye A. Detection and enrichment of

- disseminated renal carcinoma cells from peripheral blood by immunomagnetic cell separation. *Int. J. Cancer* **2001**, *92*, 577–582.
- (2) Chalmers, J. J.; Haam, S.; Zhao, Y.; McCloskey, K.; Moore, L.; Zborowski, M.; Williams, P. S. Quantification of cellular properties from external fields and resulting induced velocity: Magnetic susceptibility. *Biotechnol. Bioeng.* **1999a**, *64*, 519–526.
- (3) Chalmers, J. J.; Zhao, Y.; Nakamura, M.; Melnik, K.; Lasky, L.; Moore, L.; Zborowski, M. An instrument to determine the magnetophoretic mobility of labeled, biological cells and paramagnetic particles. *J. Magn. Magn. Mater.* **1999b**, *194*, 231–241.
- (4) Chalmers, J. J.; Zborowski, M.; Sun, L.; Moore, L. Flow through, immunomagnetic cell separation. *Biotechnol. Prog.* **1998**, *14*, 141–148.
- (5) Daugherty, P. S.; Olsen, M. J.; Iverson, B. L.; Georgiou, G. Development of an optimized expression system for the screening of antibody libraries displayed on the *Escherichia coli* surface. *Protein Eng.* **1999**, *12*, 613–21.
- (6) Gazdar, A. F.; Kurvari, V.; Virmani, A.; Gollahon, L.; Sakaguchi, M.; Westerfield, M.; Kodagoda, D.; Stasny, V.; Cunningham, H. T.; Wistuba, I. I.; Tomlinson, G.; Tonk, V.; Ashfaq, R.; Leitch, A. M.; Minna, J. D.; Shay, J. W. Characterization of paired tumor and non-tumor cell lines established from patients with breast cancer. *Int. J. Cancer* **1998**, *78*, 766–774.
- (7) Gauthier, L. R.; Granotier, C.; Soria, J. C.; Faivre, S.; Boige, V.; Raymond, E.; Boussin, F. D. Detection of circulating carcinoma cells by telomerase activity. *Br. J. Cancer* **2001**, *84*, 631–635.
- (8) Hoffman, R. A.; Houck, D. W. Cell separation using flow cytometric cell sorting. In *Cell separation methods and applications*; Recktenwald, D., Radbruch, A., Eds.; Marcel Dekker: New York, 1997; pp 237–270.
- (9) Hoyos, M.; Moore, L. R.; McCloskey, K. E.; Margel, S.; Zuberi, M.; Chalmers, J. J.; Zborowski, M. Study of magnetic particles pulse-injected into an annular SPLIT-like channel inside a quadrupole magnetic field. *J. Chromatogr., A* **2000**, *903*, 99–116.
- (10) Iinuma, H.; Okinaga, K.; Adachi, M.; Suda, K.; Sekine, T.; Sakagawa, K.; Baba, Y.; Tamura, J.; Kumagai, H.; Ida, A. Detection of tumor cells in blood using CD45 magnetic cell separation followed by nested mutant allele-specific amplification of p53 and K-ras genes in patients with colorectal cancer. *Int. J. Cancer* **2000**, *89*, 337–344.
- (11) Mavrou, A.; Coliallexi, A.; Tsangaris, G. T.; Antsaklis, A.; Panagiotopoulou, P.; Tsenghi, C.; Metaxotoy, C. Fetal cells in maternal blood: Isolation by magnetic cell sorting and confirmation by immunophenotyping and FISH. *In Vivo (Attiki)* **1998**, *12*, 195–200.
- (12) McCloskey, K.; Chalmers, J. J.; Zborowski, M. Magnetophoretic mobilities correlate to antibody binding capacities. *Cytometry* **2000**, *40*, 307–315.
- (13) Moore, L. R.; Zborowski, M.; Nakamura, M.; McCloskey, K.; Gura, S.; Lit, G.; Margel, S.; Chalmers, J. J. The use of magnetite-doped polymeric microspheres in calibrating cell tracking velocimetry. *J. Magn. Magn. Mater.* **2000**, *44*, 115–130.
- (14) Moore, L. R.; Zborowski, M.; Liping, S.; Chalmers, J. J.; Lymphocyte fractionation using immunomagnetic colloid and dipole magnet flow cell sorter. *J. Biochem. Biophys. Methods* **1998**, *37*, 11–33.
- (15) Nakamura, M.; Lasky, L.; Zborowski, M.; Chalmers, J. J. Theoretical and experimental analysis of the accuracy and reproducibility of cell tracking velocimetry. *Exp. Fluids* **2000**, *30*, 371–380.
- (16) Racila, E.; Euhus, D.; Weiss, A. J.; Rao, C.; McConnell, J.; Terstappen, L. W. M. M.; Uhr, J. W. Detection and characterization of carcinoma cells in the blood. *Proc. Natl. Acad. Sci. U.S.A.* **1998**, *95*, 4589–4594.
- (17) Safarik, I.; Safarikova, M. Use of magnetic techniques for the isolation of cells. *J. Chromatogr., B* **1999**, *722*, 33–53.
- (18) Shammo, J. M.; Smith, S. L.; Bennett, M. V.; Lee, H. W.; Ostrander, A.; Ross, A. A.; Williams, S. F. Use of a tumor-cell enrichment column for the enhanced detection of minimal residual disease in the BM or apheresis peripheral blood transplant products of breast-cancer patients. *Cytotherapy* **1999**, *5*, 367–376.
- (19) Shapiro, H. M. Flow Sorting. In *Practical Flow Cytometry*; Shapiro, H. M., Ed.; Wiley-Liss: New York, 1995; pp 217–228.
- (20) Sun, L.; Zborowski, M.; Moore, L. R.; Chalmers, J. J. Continuous, flow-through immunomagnetic cell sorting in a quadrupole field. *Cytometry* **1998**, *33*, 469–475.
- (21) Williams, P. S.; Zborowski, M.; Chalmers, J. J. Flow rate optimization for the quadrupole magnetic cell sorter. *Anal. Chem.* **1999**, *71*, 3799–3807.
- (22) Zborowski, M.; Sun, L.; Moore, L. R.; Williams, P. S.; Chalmers, J. J. Continuous cell separation using novel magnetic quadrupole flow sorter. *J. Magn. Magn. Mater.* **1999**, *194*, 224–230.

Accepted for publication September 11, 2001.

BP010109Q